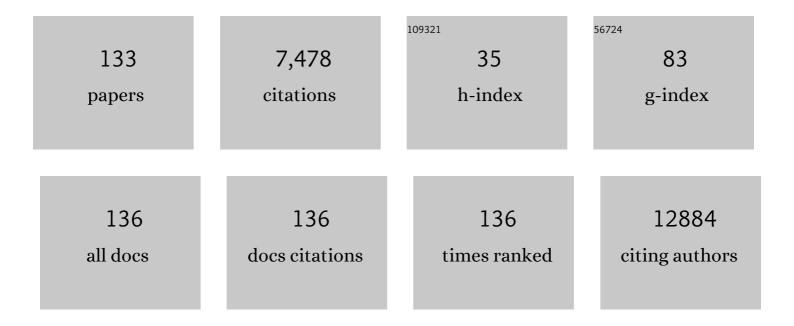
## Simon P Robinson

List of Publications by Year in descending order

Source: https://exaly.com/author-pdf/9144973/publications.pdf Version: 2024-02-01



SIMON P PORINSON

#	Article	IF	CITATIONS
1	DIPG Harbors Alterations Targetable by MEK Inhibitors, with Acquired Resistance Mechanisms Overcome by Combinatorial Inhibition. Cancer Discovery, 2022, 12, 712-729.	9.4	15
2	Hypoxia and its therapeutic possibilities in paediatric cancers. British Journal of Cancer, 2021, 124, 539-551.	6.4	28
3	TMOD-03. A NOVEL MB GR3 TRANSGENIC MOUSE MODEL IS GENERATED BY <i>MYCN</i> AND <i>P53</i> DEFECTS IN VENTRICULAR ZONE PROGENITORS Neuro-Oncology, 2021, 23, i36-i36.	1.2	0
4	Noninvasive MRI Native T1 Mapping Detects Response to <i>MYCN</i> -targeted Therapies in the Th- <i>MYCN</i> Model of Neuroblastoma. Cancer Research, 2020, 80, 3424-3435.	0.9	15
5	Infant High-Grade Gliomas Comprise Multiple Subgroups Characterized by Novel Targetable Gene Fusions and Favorable Outcomes. Cancer Discovery, 2020, 10, 942-963.	9.4	157
6	Orally bioavailable CDK9/2 inhibitor shows mechanism-based therapeutic potential in MYCN-driven neuroblastoma. Journal of Clinical Investigation, 2020, 130, 5875-5892.	8.2	40
7	MYCN expression induces replication stress and sensitivity to PARP inhibition in neuroblastoma. Oncotarget, 2020, 11, 2141-2159.	1.8	17
8	Investigating the Contribution of Collagen to the Tumor Biomechanical Phenotype with Noninvasive Magnetic Resonance Elastography. Cancer Research, 2019, 79, 5874-5883.	0.9	35
9	DIPG-25. GENETIC ALTERATIONS TARGETING THE MAPK PATHWAY CONFERS PRECLINICAL SENSITIVITY TO TRAMETINIB IN A CO-CLINICAL TRIAL IN DIPG. Neuro-Oncology, 2019, 21, ii74-ii74.	1.2	0
10	MRI Imaging of the Hemodynamic Vasculature of Neuroblastoma Predicts Response to Antiangiogenic Treatment. Cancer Research, 2019, 79, 2978-2991.	0.9	13
11	<i>In Vivo</i> Modeling of Chemoresistant Neuroblastoma Provides New Insights into Chemorefractory Disease and Metastasis. Cancer Research, 2019, 79, 5382-5393.	0.9	42
12	Imaging tumour hypoxia with oxygen-enhanced MRI and BOLD MRI. British Journal of Radiology, 2019, 92, 20180642.	2.2	111
13	Patient-derived organoids model treatment response of metastatic gastrointestinal cancers. Science, 2018, 359, 920-926.	12.6	1,199
14	Genetically modified lentiviruses that preserve microvascular function protect against late radiation damage in normal tissues. Science Translational Medicine, 2018, 10, .	12.4	15
15	Investigating Low-Velocity Fluid Flow in Tumors with Convection-MRI. Cancer Research, 2018, 78, 1859-1872.	0.9	32
16	Assessment of the direct effects of DDAH I on tumour angiogenesis in vivo. Angiogenesis, 2018, 21, 737-749.	7.2	7
17	Preclinical transgenic and patientâ€derived xenograft models recapitulate the radiological features of human adamantinomatous craniopharyngioma. Brain Pathology, 2018, 28, 475-483.	4.1	14
18	Characterisation of fibrosis in chemically-induced rat mammary carcinomas using multi-modal endogenous contrast MRI on a 1.5T clinical platform. European Radiology, 2018, 28, 1642-1653.	4.5	3

#	Article	IF	CITATIONS
19	Evaluating Imaging Biomarkers of Acquired Resistance to Targeted EGFR Therapy in Xenograft Models of Human Head and Neck Squamous Cell Carcinoma. Frontiers in Oncology, 2018, 8, 271.	2.8	9
20	Mapping Hypoxia in Renal Carcinoma with Oxygen-enhanced MRI: Comparison with Intrinsic Susceptibility MRI and Pathology. Radiology, 2018, 288, 739-747.	7.3	34
21	Abstract 4108: Longitudinal diffusion-weighted MRI assessment of NRAS mutant melanoma response to dual RAF-MEK inhibition reveals differences associated with collagen deposition. , 2018, , .		0
22	Immunoassays for the quantification of <scp>ALK</scp> and phosphorylated <scp>ALK</scp> support the evaluation of onâ€ŧarget <scp>ALK</scp> inhibitors in neuroblastoma. Molecular Oncology, 2017, 11, 996-1006.	4.6	6
23	Monitoring the Vascular Response and Resistance to Sunitinib in Renal Cell Carcinoma <i>In Vivo</i> with Susceptibility Contrast MRI. Cancer Research, 2017, 77, 4127-4134.	0.9	26
24	Noninvasive Imaging of Cycling Hypoxia in Head and Neck Cancer Using Intrinsic Susceptibility MRI. Clinical Cancer Research, 2017, 23, 4233-4241.	7.0	33
25	Correlation of Ultrasound Shear Wave Elastography with Pathological Analysis in a Xenografic Tumour Model. Scientific Reports, 2017, 7, 165.	3.3	21
26	Detecting human melanoma cell re-differentiation following BRAF or heat shock protein 90 inhibition using photoacoustic and magnetic resonance imaging. Scientific Reports, 2017, 7, 8215.	3.3	10
27	Evaluation of the Response of Intracranial Xenografts to VEGF Signaling Inhibition Using Multiparametric MRI. Neoplasia, 2017, 19, 684-694.	5.3	13
28	Pre-clinical imaging of transgenic mouse models of neuroblastoma using a dedicated 3-element solenoid coil on a clinical 3T platform. British Journal of Cancer, 2017, 117, 791-800.	6.4	9
29	Imaging biomarker roadmap for cancer studies. Nature Reviews Clinical Oncology, 2017, 14, 169-186.	27.6	792
30	Multi-Channel Optical Coherence Elastography Using Relative and Absolute Shear-Wave Time of Flight. PLoS ONE, 2017, 12, e0169664.	2.5	4
31	PCM-08IN VIVOMAGNETIC RESONANCE IMAGING IDENTIFIES CLINICAL PHENOTYPES OF PAEDIATRIC GLIOBLASTOMA IN AN ORTHOTOPIC MOUSE XENOGRAFT MODEL. Neuro-Oncology, 2016, 18, iii140.4-iii141.	1.2	0
32	Modulation of renal oxygenation and perfusion in rat kidney monitored by quantitative diffusion and blood oxygen level dependent magnetic resonance imaging on a clinical 1.5T platform. BMC Nephrology, 2016, 17, 142.	1.8	6
33	Multiparameter Lead Optimization to Give an Oral Checkpoint Kinase 1 (CHK1) Inhibitor Clinical Candidate: ( <i>R</i> )-5-((4-((Morpholin-2-ylmethyl)amino)-5-(trifluoromethyl)pyridin-2-yl)amino)pyrazine-2-carbonitrile (CCT245737), Journal of Medicinal Chemistry, 2016, 59, 5221-5237.	6.4	24
34	Repeatability and sensitivity of measurements in patients with head and neck squamous cell carcinoma at 3T. Journal of Magnetic Resonance Imaging, 2016, 44, 72-80.	3.4	27
35	Investigating intracranial tumour growth patterns with multiparametric MRI incorporating Gdâ€DTPA and USPIOâ€enhanced imaging. NMR in Biomedicine, 2016, 29, 1608-1617.	2.8	11
36	Acute tumour response to a bispecific Ang-2-VEGF-A antibody: insights from multiparametric MRI and gene expression profiling. British Journal of Cancer, 2016, 115, 691-702.	6.4	19

#	Article	IF	CITATIONS
37	HG-99A PATIENT-DERIVED PAEDIATRIC HIGH GRADE GLIOMA AND DIPG CELL CULTURE PANEL RECAPITULATING THE GENOTYPIC AND PHENOTYPIC DIVERSITY OF THE DISEASE. Neuro-Oncology, 2016, 18, iii71.3-iii71.	1.2	0
38	Investigating the Vascular Phenotype of Subcutaneously and Orthotopically Propagated PC3 Prostate Cancer Xenografts Using Combined Carbogen Ultrasmall Superparamagnetic Iron Oxide MRI. Topics in Magnetic Resonance Imaging, 2016, 25, 237-243.	1.2	5
39	Investigating the role of tumour cell derived i <scp>NOS</scp> on tumour growth and vasculature <i>in vivo</i> using a tetracycline regulated expression system. International Journal of Cancer, 2016, 138, 2678-2687.	5.1	15
40	p53 Loss in MYC-Driven Neuroblastoma Leads to Metabolic Adaptations Supporting Radioresistance. Cancer Research, 2016, 76, 3025-3035.	0.9	33
41	Oxygen-Enhanced MRI Accurately Identifies, Quantifies, and Maps Tumor Hypoxia in Preclinical Cancer Models. Cancer Research, 2016, 76, 787-795.	0.9	133
42	Inhibition of mTOR-kinase destabilizes MYCN and is a potential therapy for MYCN-dependent tumors. Oncotarget, 2016, 7, 57525-57544.	1.8	42
43	Apparent diffusion coefficient is highly reproducible on preclinical imaging systems: Evidence from a sevenâ€center multivendor study. Journal of Magnetic Resonance Imaging, 2015, 42, 1759-1764.	3.4	15
44	Rapid modification of the bone microenvironment following short-term treatment with Cabozantinib in vivo. Bone, 2015, 81, 581-592.	2.9	33
45	Combined MYC and P53 Defects Emerge at Medulloblastoma Relapse and Define Rapidly Progressive, Therapeutically Targetable Disease. Cancer Cell, 2015, 27, 72-84.	16.8	165
46	Cyclin-Dependent Kinase Inhibitor AT7519 as a Potential Drug for MYCN-Dependent Neuroblastoma. Clinical Cancer Research, 2015, 21, 5100-5109.	7.0	49
47	Detecting microvascular changes in the mouse spleen using optical computed tomography. Microvascular Research, 2015, 101, 96-102.	2.5	2
48	Exploring the Biomechanical Properties of Brain Malignancies and Their Pathologic Determinants <i>In Vivo</i> with Magnetic Resonance Elastography. Cancer Research, 2015, 75, 1216-1224.	0.9	90
49	Abstract 1488:In vivomagnetic resonance elastography in pediatric brain tumor models. , 2015, , .		2
50	Abstract 3271: Novel orthotopic pediatric high grade glioma xenografts evaluated with magnetic resonance imaging mimic human disease. Cancer Research, 2015, 75, 3271-3271.	0.9	2
51	Abstract 1372: Acquired resistance to sunitinib is not associated with functional re-vascularization in 786-O renal cell carcinoma xenografts. , 2015, , .		0
52	Abstract 2930: Differential tumour response to birinapant and irinotecan revealed by non-invasive MRI. , 2015, , .		0
53	Abstract 491: Tumor response to cabozantinib in the TH-MYCN GEM model of neuroblastoma. , 2015, , .		0
54	Reduced Warburg Effect in Cancer Cells Undergoing Autophagy: Steady- State 1H-MRS and Real-Time Hyperpolarized 13C-MRS Studies. PLoS ONE, 2014, 9, e92645.	2.5	17

#	Article	IF	CITATIONS
55	Tumour biomechanical response to the vascular disrupting agent ZD6126 in vivo assessed by magnetic resonance elastography. British Journal of Cancer, 2014, 110, 1727-1732.	6.4	48
56	Non-invasive molecular profiling of cancer using photoacoustic imaging of functionalized gold nanorods. , 2014, , .		1
57	Preclinical Evaluation of Imaging Biomarkers for Prostate Cancer Bone Metastasis and Response to Cabozantinib. Journal of the National Cancer Institute, 2014, 106, dju033.	6.3	59
58	Detection of the Prodrug-Activating Enzyme Carboxypeptidase G2 Activity with Chemical Exchange Saturation Transfer Magnetic Resonance. Molecular Imaging and Biology, 2014, 16, 152-157.	2.6	18
59	Intrinsic Susceptibility MRI Identifies Tumors with ALKF1174L Mutation in Genetically-Engineered Murine Models of High-Risk Neuroblastoma. PLoS ONE, 2014, 9, e92886.	2.5	16
60	Abstract LB-201: MYC and TP53 defects interact at medulloblastoma relapse to define rapidly progressive disease and can be targeted therapeutically. , 2014, , .		0
61	Evaluation and Immunohistochemical Qualification of Carbogen-Induced ΔR2* as a Noninvasive Imaging Biomarker of Improved Tumor Oxygenation. International Journal of Radiation Oncology Biology Physics, 2013, 87, 160-167.	0.8	14
62	Critical research gaps and translational priorities for the successful prevention and treatment of breast cancer. Breast Cancer Research, 2013, 15, R92.	5.0	320
63	Acute tumour response to the MEK1/2 inhibitor selumetinib (AZD6244, ARRY-142886) evaluated by non-invasive diffusion-weighted MRI. British Journal of Cancer, 2013, 109, 1562-1569.	6.4	22
64	Small Molecule Inhibitors of Aurora-A Induce Proteasomal Degradation of N-Myc in Childhood Neuroblastoma. Cancer Cell, 2013, 24, 75-89.	16.8	240
65	Evaluation of Clinically Translatable MR Imaging Biomarkers of Therapeutic Response in the TH-MYCNTransgenic Mouse Model of Neuroblastoma. Radiology, 2013, 266, 130-140.	7.3	33
66	1 H NMR and hyperpolarized 13 C NMR assays of pyruvate–lactate: a comparative study. NMR in Biomedicine, 2013, 26, 1321-1325.	2.8	25
67	Exploring ΔR <sub>2</sub> * and ΔR <sub>1</sub> as imaging biomarkers of tumor oxygenation. Journal of Magnetic Resonance Imaging, 2013, 38, 429-434.	3.4	44
68	Model Free Approach to Kinetic Analysis of Real-Time Hyperpolarized 13C Magnetic Resonance Spectroscopy Data. PLoS ONE, 2013, 8, e71996.	2.5	134
69	Characterization of a Novel Mouse Model of Multiple Myeloma and Its Use in Preclinical Therapeutic Assessment. PLoS ONE, 2013, 8, e57641.	2.5	21
70	A Multi-Parametric Imaging Investigation of the Response of C6 Glioma Xenografts to MLN0518 (Tandutinib) Treatment. PLoS ONE, 2013, 8, e63024.	2.5	10
71	Abstract 3924: Multimodality imaging investigation of response to cabozantinib in a VCaP model of prostate bone metastasis , 2013, , .		0
72	Abstract 1559: Evaluation of MR imaging biomarkers of the vascular and infiltrative phenotype in intracranial MDA-MB-231 tumors , 2013, , .		0

#	Article	IF	CITATIONS
73	Abstract 4459: Evaluating imaging biomarkers of acquired resistance to targeted EGFR therapy in xenograft models of human squamous cell carcinoma of the head and neck (SCCHN) , 2013, , .		2
74	Abstract 5037: Intrinsic susceptibility magnetic resonance imaging identifies tumors with ALKF1174L mutation in transgenic murine models of high-risk neuroblastoma , 2013, , .		0
75	CCT244747 Is a Novel Potent and Selective CHK1 Inhibitor with Oral Efficacy Alone and in Combination with Genotoxic Anticancer Drugs. Clinical Cancer Research, 2012, 18, 5650-5661.	7.0	84
76	False-negative MRI biomarkers of tumour response to targeted cancer therapeutics. British Journal of Cancer, 2012, 106, 1960-1966.	6.4	10
77	Dependence of Wilms tumor cells on signaling through insulin-like growth factor 1 in an orthotopic xenograft model targetable by specific receptor inhibition. Proceedings of the National Academy of Sciences of the United States of America, 2012, 109, E1267-76.	7.1	31
78	MRI measurements of vessel calibre in tumour xenografts: Comparison with vascular corrosion casting. Microvascular Research, 2012, 84, 323-329.	2.5	16
79	Evaluation of novel combined carbogen USPIO (CUSPIO) imaging biomarkers in assessing the antiangiogenic effects of cediranib (AZD2171) in rat C6 gliomas. International Journal of Cancer, 2012, 131, 1854-1862.	5.1	9
80	The ALKF1174L Mutation Potentiates the Oncogenic Activity of MYCN in Neuroblastoma. Cancer Cell, 2012, 22, 117-130.	16.8	270
81	Nonâ€invasive <i>in vivo</i> imaging of vessel calibre in orthotopic prostate tumour xenografts. International Journal of Cancer, 2012, 130, 1284-1293.	5.1	19
82	The Aurora Kinase Inhibitor CCT137690 Downregulates MYCN and Sensitizes <i>MYCN</i> -Amplified Neuroblastoma <i>In Vivo</i> . Molecular Cancer Therapeutics, 2011, 10, 2115-2123.	4.1	79
83	Immunohistochemical assessment of intrinsic and extrinsic markers of hypoxia in reproductive tissue: differential expression of HIF1α and HIF2α in rat oviduct and endometrium. Journal of Molecular Histology, 2011, 42, 341-354.	2.2	14
84	Active site mutant dimethylarginine dimethylaminohydrolase 1 expression confers an intermediate tumour phenotype in C6 gliomas. Journal of Pathology, 2011, 225, 344-352.	4.5	27
85	Improving apparent diffusion coefficient estimates and elucidating tumor heterogeneity using Bayesian adaptive smoothing. Magnetic Resonance in Medicine, 2011, 65, 438-447.	3.0	24
86	Investigating temporal fluctuations in tumor vasculature with combined carbogen and ultrasmall superparamagnetic iron oxide particle (CUSPIO) imaging. Magnetic Resonance in Medicine, 2011, 66, 227-234.	3.0	11
87	Noninvasive detection of carboxypeptidase G2 activity <i>in vivo</i> . NMR in Biomedicine, 2011, 24, 343-350.	2.8	11
88	Abstract 4074: The effects of the HIF pathway inhibitor NSC-134754 on glucose metabolism. , 2011, , .		0
89	Abstract 3788: Autophagy induced by DCA, PI3K inhibition or starvation results in reduced lactate production measured in real-time by DNP 13C MRS. , 2011, , .		0
90	Abstract 5290: Imaging biomarkers of response to chemotherapy in neuroblastoma. , 2011, , .		0

#	Article	IF	CITATIONS
91	Abstract 4345: AZD8055, a combined TORC1/TORC2 inhibitor regulates Mycn protein expression and prevents neuroblastoma growth in vitro and in vivo. , 2011, , .		Ο
92	Bayesian estimation of changes in transverse relaxation rates. Magnetic Resonance in Medicine, 2010, 64, 914-921.	3.0	28
93	Intrinsic Susceptibility MR Imaging of Chemically Induced Rat Mammary Tumors: Relationship to Histologic Assessment of Hypoxia and Fibrosis. Radiology, 2010, 254, 110-118.	7.3	72
94	Lessons from Animal Imaging in Preclinical Models. , 2010, , 95-116.		1
95	Abstract 4189: Characterization of tumor progression and chemoresponse in a novel transgenic mouse model of neuroblastoma (TH-MYCN) using magnetic resonance imaging. , 2010, , .		Ο
96	Robust estimation of the apparent diffusion coefficient (ADC) in heterogeneous solid tumors. Magnetic Resonance in Medicine, 2009, 62, 420-429.	3.0	50
97	Hyperpolarized <sup>13</sup> C magnetic resonance detection of carboxypeptidase G2 activity. Magnetic Resonance in Medicine, 2009, 62, 1300-1304.	3.0	36
98	Abstract B257: Chronic dosing with MLN0518 (Tandutinib), a small molecule PDGFRα/β inhibitor, reduces tumor growth, hypoxia, and perfusion in C6 glioma xenografts: An investigation using immunohistochemical and MRI methods. , 2009, , .		0
99	Abstract C90: An MRI and histological investigation of the acute response of orthotopic PC3 prostate tumors to the HIF pathway inhibitor NSCâ€134754in vivo. , 2009, , .		0
100	The effects of tumorâ€derived plateletâ€derived growth factor on vascular morphology and function <i>in vivo</i> revealed by susceptibility MRI. International Journal of Cancer, 2008, 122, 1548-1556.	5.1	23
101	Effect of Gdâ€ÐTPAâ€BMA on choline signals of HT29 tumors detected by in vivo <sup>1</sup> H MRS. Journal of Magnetic Resonance Imaging, 2008, 28, 1201-1208.	3.4	17
102	Longitudinal in vivo susceptibility contrast MRI measurements of LS174T colorectal liver metastasis in nude mice. Journal of Magnetic Resonance Imaging, 2008, 28, 1451-1458.	3.4	19
103	Vessel Size Index Magnetic Resonance Imaging to Monitor the Effect of Antivascular Treatment in a Rodent Tumor Model. International Journal of Radiation Oncology Biology Physics, 2008, 71, 1470-1476.	0.8	27
104	Susceptibility Contrast Magnetic Resonance Imaging Determination of Fractional Tumor Blood Volume: A Noninvasive Imaging Biomarker of Response to the Vascular Disrupting Agent ZD6126. International Journal of Radiation Oncology Biology Physics, 2007, 69, 872-879.	0.8	26
105	Assessment of Tumor Response to the Vascular Disrupting Agents 5,6-Dimethylxanthenone-4-Acetic Acid or Combretastatin-A4-Phosphate by Intrinsic Susceptibility Magnetic Resonance Imaging. International Journal of Radiation Oncology Biology Physics, 2007, 69, 1238-1245.	0.8	15
106	Hypoxia: Importance in tumor biology, noninvasive measurement by imaging, and value of its measurement in the management of cancer therapy. International Journal of Radiation Biology, 2006, 82, 699-757.	1.8	561
107	Rat Tumor Response to the Vascular-Disrupting Agent 5,6-Dimethylxanthenone-4-Acetic Acid as Measured by Dynamic Contrast-Enhanced Magnetic Resonance Imaging, Plasma 5-Hydroxyindoleacetic Acid Levels, and Tumor Necrosis. Neoplasia, 2006, 8, 199-206.	5.3	35
108	The Response of RIF-1 Fibrosarcomas to the Vascular-Disrupting Agent ZD6126 Assessed by In Vivo and Ex Vivo1H Magnetic Resonance Spectroscopy. Neoplasia, 2006, 8, 560-567.	5.3	36

#	Article	IF	CITATIONS
109	Tumour overexpression of inducible nitric oxide synthase (iNOS) increases angiogenesis and may modulate the anti-tumour effects of the vascular disrupting agent ZD6126. Microvascular Research, 2006, 71, 76-84.	2.5	32
110	A Longitudinal Study of R2* and R2 Magnetic Resonance Imaging Relaxation Rate Measurements in Murine Liver After a Single Administration of 3 Different Iron Oxide-Based Contrast Agents. Investigative Radiology, 2005, 40, 784-791.	6.2	32
111	The Effects of Tumour Blood Flow and Oxygenation Modifiers on Subcutaneous Tumours as Determined by NIRS. , 2005, 566, 75-81.		6
112	Tumor Dose Response to the Vascular Disrupting Agent, 5,6-Dimethylxanthenone-4-Acetic Acid, Using In vivo Magnetic Resonance Spectroscopy. Clinical Cancer Research, 2005, 11, 3705-3713.	7.0	33
113	Acute Tumor Response to ZD6126 Assessed by Intrinsic Susceptibility Magnetic Resonance Imaging. Neoplasia, 2005, 7, 466-474.	5.3	32
114	Orally administered lenalidomide (CC-5013) is anti-angiogenic in vivo and inhibits endothelial cell migration and Akt phosphorylation in vitro. Microvascular Research, 2005, 69, 56-63.	2.5	254
115	Current issues in the utility of 19 F nuclear magnetic resonance methodologies for the assessment of tumour hypoxia. Philosophical Transactions of the Royal Society B: Biological Sciences, 2004, 359, 987-996.	4.0	49
116	Tumor R2* is a prognostic indicator of acute radiotherapeutic response in rodent tumors. Journal of Magnetic Resonance Imaging, 2004, 19, 482-488.	3.4	91
117	In vivo determination of tumor oxygenation during growth and in response to carbogen breathing using 15C5-loaded alginate capsules as fluorine-19 magnetic resonance imaging oxygen sensors. International Journal of Radiation Oncology Biology Physics, 2004, 60, 909-919.	0.8	28
118	Single Dose of the Antivascular Agent, ZD6126 (N-Acetylcoichinol-O-Phosphate), Reduces Perfusion for at Least 96 Hours in the GH3 Prolactinoma Rat Tumor Model. Neoplasia, 2004, 6, 150-157.	5.3	34
119	Overexpression of Dimethylarginine Dimethylaminohydrolase Enhances Tumor Hypoxia: An Insight into the Relationship of Hypoxia and Angiogenesis In Vivo. Neoplasia, 2004, 6, 401-411.	5.3	25
120	Tumor vascular architecture and function evaluated by non-invasive susceptibility MRI methods and immunohistochemistry. Journal of Magnetic Resonance Imaging, 2003, 17, 445-454.	3.4	130
121	Tumour dose response to the antivascular agent ZD6126 assessed by magnetic resonance imaging. British Journal of Cancer, 2003, 88, 1592-1597.	6.4	114
122	Issues in GRE & Se Magnetic Resonance Imaging to Probe Tumor Oxygenation. Advances in Experimental Medicine and Biology, 2003, 530, 441-448.	1.6	6
123	Effects of overexpression of dimethylarginine dimethylaminohydrolase on tumor angiogenesis assessed by susceptibility magnetic resonance imaging. Cancer Research, 2003, 63, 4960-6.	0.9	57
124	Enhanced Uptake of Ifosfamide into GH3 Prolactinomas with Hypercapnic Hyperoxic Gases Monitored In Vivo by 31P MRS. Neoplasia, 2002, 4, 539-543.	5.3	11
125	The importance of tumor metabolism in cancer prognosis and therapy; pre-clinical studies on rodent tumors with agents that improve tumor oxygenation. Advances in Enzyme Regulation, 2002, 42, 131-141.	2.6	5
126	Effects of different levels of hypercapnic hyperoxia on tumour R 2 â^— and arterial blood gases. Magnetic Resonance Imaging, 2001, 19, 161-166.	1.8	41

#	Article	IF	CITATIONS
127	Applications of Magnetic Resonance in Model Systems: Tumor Biology and Physiology. Neoplasia, 2000, 2, 139-151.	5.3	110
128	Tumour response to hypercapnia and hyperoxia monitored by FLOOD magnetic resonance imaging. NMR in Biomedicine, 1999, 12, 98-106.	2.8	78
129	Tumour response to hypercapnia and hyperoxia monitored by FLOOD magnetic resonance imaging. NMR in Biomedicine, 1999, 12, 98-106.	2.8	1
130	Magnetic resonance imaging techniques for monitoring changes in tumor oxygenation and blood flow. Seminars in Radiation Oncology, 1998, 8, 197-207.	2.2	78
131	The response of human tumors to carbogen breathing, monitored by gradient-recalled echo magnetic resonance imaging. International Journal of Radiation Oncology Biology Physics, 1997, 39, 697-701.	0.8	128
132	Modification of Tumour Perfusion and Oxygenation Monitored by Gradient Recalled Echo MRI and31P MRS. , 1996, 9, 208-216.		27
133	Noninvasive monitoring of carbogen-induced changes in tumor blood flow and oxygenation by functional magnetic resonance imaging. International Journal of Radiation Oncology Biology Physics, 1995, 33, 855-859	0.8	113